

# Impuriton-Phonon Quasiparticles Possibility and Rapid Dissolution of $^3\text{He}$ Inclusions in $^4\text{He}$ Crystal

Victor Lykah<sup>1\*</sup> and Eugene Syrkin<sup>21</sup>

<sup>1</sup>Department of Physics and Technology, NTU "Kharkiv Polytechnic Institute", Kharkiv, Ukraine

<sup>2</sup>Theoretical Department, B.I. Verkin Institute of Low Temperature Physics of the NASU, Kharkiv, Ukraine

Email: lykahva@yahoo.com Email: syrkin@ilt.kharkov.ua

**Abstract** The properties of quantum solid solutions are investigated theoretically taking into account the interaction between waves of different nature: phonons and impuritons. The wave's interaction leads to a nonlinear Schrodinger equation that describes soliton - the impuriton-phonon, a new quasiparticle. As shown, the impuriton-phonons have velocity comparable to sound speed. Under heat step at the inclusion-matrix boundary a chemical potential step is formed. This leads to transition of  $^3\text{He}$  atoms into the matrix with one of the following mechanisms: (i) phonon emission and band movement of the impuriton; (ii) threshold emission of the impuriton-phonon (the photoelectric effect analogy). It is shown that the narrow impuriton band cannot describe the rapid movement of the impuriton-phonon quasiparticle; alternative descriptions, channeling and induced transformation of the band, are proposed. It qualitatively explains the experiments with rapid dissolution of the  $^3\text{He}$  phase inclusion in the  $^4\text{He}$  matrix.

**Keywords:** Solid helium, quantum tunneling of defects, matter waves, phonon interactions with other quasi-particles.

## 1 Introduction

Quantum solutions  $^3\text{He}$ - $^4\text{He}$  demonstrate unusual set of properties in the crystalline state [1]. In solid helium existence of specific quasiparticles, defectons (point defect in the  $^4\text{He}$  matrix), was predicted in [2]. Impuritons (light impurity  $^3\text{He}$  atom in the  $^4\text{He}$  matrix), and vacancions (vacancies in the  $^4\text{He}$  matrix) are the defectons. The impuritons were found in experiment [3]. In the classic crystal, diffusion takes place by rare jumps between neighboring sites [4,5]. In quantum  $^4\text{He}$  crystal the impurities and the vacancies are delocalized due to quantum tunneling. Band motion of the defectons is possible similarly to electron motion in the conduction band [2,4]. It is also known as "mass fluctuation waves" [6].

Quantum diffusion of  $^3\text{He}$  impuritons in solid  $^4\text{He}$  was found, see [7,8]. In solid solutions at low temperatures, the nucleation of a new  $^3\text{He}$  phase in the  $^4\text{He}$  matrix leads to a new quantum transport phenomena that have been studied experimentally (see review [8]). Special interest is the rapid dissolution (fast decay) of the  $^3\text{He}$  phase nucleation under heating above the phase separation on  $T - x$  diagram. This is a threshold effect: in the case of overheating  $\Delta T > \Delta T_c = 25\text{mK}$  (close to the point  $T_i = 100\text{mK}$ ,  $x = 3 - 4\%$ ) dissolution rate of the nucleation increases by several orders of magnitude [9,10,11]. Here  $T$  and  $x$  are temperature and the  $^3\text{He}$  concentration. This threshold effect cannot be explained within the frames of the existing theory of quantum diffusion in volume [12,13] and in twin boundary [14].

Vacancion-phonon interaction was considered as one of the alternative explanations of an unusual phonon dispersion law found in neutron diffraction experiments in  $^4\text{He}$  [15]. Vacancion-phonon Interaction was theoretically investigated in [16,17,18]. Impuriton-phonon interaction (scattering) was found in the experiment [19].

In this paper, the interaction of sound waves and impuritons and its role in the very rapid dissolution of nuclei in the quantum solid solutions  $^3\text{He}$ - $^4\text{He}$  are investigated. We introduce a new quasiparticle, impuriton-phonon, which moves at high velocity (comparable to the sound speed). The new quasiparticle allows us to describe the very rapid dissolution of the nuclei in the solid solutions of quantum crystals  $^3\text{He}$ - $^4\text{He}$ .

The paper consists of the following sections. The second section deals with the properties of non-interacting impuritons and phonons; equations which take into account their interaction are obtained. In

the third section the new quasiparticle impuriton-phonon is introduced. In the fourth section, dynamics of chemical potentials in different phases is considered as the driving force of the transition and rapid dissolution under the overheating. In the fifth section, different mechanisms of  $^3\text{He}$  atoms transition from the nucleation into the matrix are investigated, the threshold generation mechanism of the impuriton-phonon quasiparticles is described; the experimental and theoretical parameters are related. Photoelectric effect analogy with the threshold generation mechanism of the impuriton-phonon quasiparticle is analyzed in the sixth section. In the seventh section, the theoretical model parameters are estimated from the experimental data; the applicability of the approximations and analogies with other quasi-particles are discussed; high-velocity is obtained. In the conclusion section, the main results are summarized briefly.

## 2 Lattice and Impuritons Subsystems and Their Interaction

Lagrangian of the system is:

$$L = L_L + L_{Imp} + L_{int}. \quad (1)$$

Here  $L_L$ ,  $L_{Imp}$ , and  $L_{int}$  describe lattice, impurities, and their interaction, respectively.

### 2.1 Lattice Elasticity and Vibrational Spectrum

Long-wave description of the displacements in the crystal coincides with the dynamic equations of elasticity theory [4]. Stress and strain states of a crystal in the presence of external forces are defined by dynamic equations for elastic medium [4]

$$\rho \frac{\partial^2 u_i}{\partial t^2} = \nabla_k \sigma_{ki} + f_i. \quad (2)$$

where  $u$  is displacement vector,  $\rho = m/V_0$  is average mass density of the crystal ( $V_0$  is the unit cell volume),  $\sigma_{ik}$  is symmetric stress tensor, vector  $f$  is average density of external forces acting on the crystal. If the crystal deformation is purely elastic, then the stress is linearly proportional to the strain (deformations)  $\epsilon_{ik}$  by the generalized Hooke's law  $\sigma_{ik} = \lambda_{iklm} \epsilon_{lm}$ , where  $\lambda_{iklm}$  is tensor of the elastic moduli and  $\epsilon_{ik} = (\nabla_i u_k + \nabla_k u_i)/2$  is linear strain tensor. A complex stress state of the crystal is described by the average hydrostatic pressure [4]:

$$p_0 = -\frac{1}{3} \sigma_{kk} \quad (3)$$

The free elastic field ( $f = 0$ ) is described by the dynamic equation

$$\rho \frac{\partial^2 u_i}{\partial t^2} - \lambda_{iklm} \nabla_k \nabla_l u_m = 0. \quad (4)$$

Solid  $^4\text{He}$  needs static pressure  $p \geq 25\text{bar}$ ) or  $f = \text{const}$ , so equation (4) needs renormalization.

In the isotropic approximation the elastic moduli tensor  $\lambda_{iklm}$  is reduced to two independent modules [20]:

$$\lambda_{iklm} = \lambda \delta_{ik} \delta_{lm} + G(\delta_{il} \delta_{km} + \delta_{im} \delta_{kl}). \quad (5)$$

where  $G$  and  $\lambda$  are shear modulus and Lamé coefficient of the elastic medium. Isotropic elastic field has two characteristic wave velocities: longitudinal  $c_l$  and transverse  $c_t$  ones [4,20]:

$$c_l^2 = \frac{3K + 4G}{3\rho}; \quad c_t^2 = \frac{G}{\rho}. \quad (6)$$

Here  $K = \lambda + \frac{2}{3}G$  is hydrostatic compression modulus in an isotropic medium. We note that from equations (3, 5) one can get a clear relationship between the average hydrostatic pressure  $p_0$  and the relative compression of an isotropic medium or a cubic crystal:  $\sigma_{ll} = 3K\epsilon_{ll}$ . Cubic and hexagonal crystals are isotropic if their anisotropy parameters are [21,22]

$$A_{cub} = \frac{2c_{44}}{c_{11} - c_{12}}, \quad A_{hex} = \frac{\sqrt{c_{11}c_{33}} - c_{13}}{2c_{55}}, \quad (7)$$

are close to 1. Here  $c_{ik}$  are components of the elastic moduli tensor  $\lambda_{iklm}$  in Voigt notation accounting for the crystal symmetry [20], and  $c_{55} = c_{44}$ . Substituting the values  $c_{11}/\rho = 3.66 \cdot 10^9 (\text{cm/s})^2$ ;  $c_{13}/\rho = 0.954 \cdot 10^9 (\text{cm/s})^2$ ;  $c_{33}/\rho = 4.72 \cdot 10^9 (\text{cm/s})^2$ ;  $c_{44}/\rho = 0.944 \cdot 10^9 (\text{cm/s})^2$  from [1] we obtain  $A_{hex} = A_{hcp} = 1.696$ , for molar volume  $19.8 \text{cm}^3/\text{mole}$ . When molar volume is  $20.97 \text{cm}^3/\text{mole}$ , which is closer to the experiment [11], we have  $c_{11}/\rho = 2.12 \cdot 10^9 (\text{cm/s})^2$ ;  $c_{13}/\rho = 0.549 \cdot 10^9 (\text{cm/s})^2$ ;  $c_{33}/\rho = 2.90 \cdot 10^9 (\text{cm/s})^2$ ;  $c_{44}/\rho = 0.652 \cdot 10^9 (\text{cm/s})^2$  according to [1] and  $A_{hex} = A_{hcp} = 1.481$ . For comparison, we have  $A_{cub} = A_{bcc} = 23.6$  in solid bcc  ${}^3\text{He}$  at a molar volume of  $21.64 \text{cm}^3/\text{mole}$  [1]. Consequently, the phase hcp  ${}^4\text{He}$  is close to isotropic.

In an isotropic medium, using (5, 6), the Lagrangian and dynamic equation (4) can be simplified:

$$L = \int \left( \frac{1}{2} \rho \left( \frac{\partial \mathbf{u}}{\partial t} \right)^2 - \frac{1}{2} \rho c_l^2 \left( \frac{\partial u_i}{\partial x_i} \right)^2 \right) dV. \quad (8)$$

$$\rho \frac{\partial^2 \mathbf{u}}{\partial t^2} - \rho c_l^2 \Delta \mathbf{u} = 0, \quad (9)$$

where  $\Delta$  is Laplace operator. This equation describes the propagation of waves with an acoustic dispersion law:

$$\omega = c_l k. \quad (10)$$

The longitudinal velocity of sound  $c_l = 400 \div 600 \text{m/s}$  [1] depends on the pressure and the  ${}^4\text{He}$  crystal orientation. In the case of quantization of the acoustic field the phonons energy has the form

$$\varepsilon = \hbar \omega, \quad (11)$$

where  $\hbar$  is Planck's constant.

## 2.2 The Impuriton Spectrum and Hamiltonian

In quantum crystal, due to quantum tunneling, a defect is delocalized i.e. a quasiparticle defecton exists [2,4]. The defecton energy  $\varepsilon_D(\mathbf{k})$  can be obtained, if the energy of the defect-free crystal is subtracted of the energy of the defected crystal. The probability of quantum tunneling of the defecton is relatively small, so we can use the strong coupling approximation known in the electronic theory [5,23,24]. For a simple cubic lattice we have the dispersion law of the defecton is

$$\varepsilon_D(\mathbf{k}) = \varepsilon_0 + \varepsilon_1 (\cos k a_1 + \cos k a_2 + \cos k a_3), \quad (12)$$

where  $\varepsilon_0, \varepsilon_1$  are constants ( $|\varepsilon_1|$  is proportional to the probability of quantum tunneling)  $a_\alpha$  are lattice translational vectors. Defectons are light quasiparticles, as compared with the matrix atoms, so the dispersion law has maximum at  $\mathbf{k} = 0$  and  $\varepsilon_1 > 0$  in (12). The half-width of the defecton energy band is  $\Delta\varepsilon = 3|\varepsilon_1|$ . According to experiments in solid  ${}^4\text{He}$ , energy bandwidth is  $\Delta\varepsilon \sim 1\text{K} \sim 10^{-23}\text{J}$  for "vacacion" and  $\Delta\varepsilon \sim (10^{-5} \div 10^{-4})\text{K} \sim (10^{-28} \div 10^{-27})\text{J}$  for  ${}^3\text{He}$  "Impuriton". The formation energies for vacacion ( $\varepsilon_0 \simeq 5\text{K}$ ) and impuriton ( $\varepsilon_0 \simeq 0.2\text{K}$ ) also differ considerably. In the isotropic approximation the expansion (12) around the maximum value  $\varepsilon(k)$  (the band top) has the form

$$\varepsilon_D = \varepsilon_0 + \Delta\varepsilon + \frac{\hbar^2 k^2}{2m^*}, \quad m^* = -\frac{\hbar^2}{a^2 \varepsilon_1}, \quad (13)$$

where  $m^* < 0$  is defecton's effective mass. This dispersion law has a maximum at  $k = 0$  so the defecton moves more like a hole not an electron [5,23,24]. According to (13) the defecton effective mass estimation is following:  $m^* = -6,58 \cdot 10^{-23}\text{kg} < 0$ . Electrons with the dispersion law (12) can be described by the equivalent Hamiltonian [23] (chapter 6), [24], which is obtained in the Wannier representation by method of slowly changing potentials. In this method, an analytical continuous function  $\varepsilon(\mathbf{k})$  of the quasi-wave vector  $\mathbf{k}$  is replaced by the same function  $\varepsilon(-i\nabla)$  of operator  $(-i\nabla)$ . Then Schrodinger equation

$$\hat{H}\psi(\mathbf{r}, t) = i\hbar \frac{\partial}{\partial t} \psi(\mathbf{r}, t); \quad \hat{H} = \hat{K} + \hat{U}. \quad (14)$$

is replaced with an equation based on the equivalent Hamiltonian:

$$\varepsilon_n(-i\nabla)f_n(\mathbf{r}, t) + U(\mathbf{r})f_n(\mathbf{r}, t) = i\hbar \frac{\partial}{\partial t} f_n(\mathbf{r}, t). \quad (15)$$

Here  $\mathbf{r}$  are coordinates of lattice sites,  $f_n(\mathbf{r}, t)$  play role of the wave functions in the local potential field  $U(\mathbf{r})$ , which is weak and slowly varying in space,  $n$  is the band number. The equivalent hamiltonian method considers a quasiparticle to be free with altered kinetic energy operator  $\hat{K} = \varepsilon_n(-i\nabla)$  instead of the original particle placed in an ideal lattice [23,24]. The defecton's dispersion law (12) is obtained by setting  $U(\mathbf{r}) = 0$  in the Schrodinger equation (15) and applying the Fourier transform.

Dispersion laws for phonon (10) and impuriton (12) can be written in the same form. Then, in the 1D case, the dispersion law (12) can be written for frequencies as:

$$\omega(k) = \omega_0 + \omega_1 \cos ka; \quad \omega_0 = \frac{\varepsilon_0}{\hbar}; \quad \omega_1 = \frac{\varepsilon_1}{\hbar}. \quad (16)$$

Group velocity of an impuriton is:

$$v_g(k) = \left| \frac{\partial \omega(k)}{\partial k} \right| = \left| \frac{\varepsilon_1 a}{\hbar} \sin ka \right| \simeq \frac{\varepsilon_1 a}{\hbar}. \quad (17)$$

Usually, for its evaluation rather large value  $k \simeq 1/a$  is taken. So, taking  $a \simeq 0.38$  nm and  $\varepsilon_1 \sim 10^{-28}$  J we obtain the estimation  $v_g(k) \sim 10^{-4}$  m/s [2,4].

### 2.3 Impuriton-Lattice Interaction.

The quantum helium crystals are characterized by high zero-point oscillations. If a quantum atomic oscillator has parameters  $k$  (stiffness of a potential) and  $m$  (atomic mass), its ground state energy is  $\hbar\omega/2 = kx_0^2/2$ . An amplitude of the zero-point oscillations can be estimated as  $x_0 \simeq \hbar^{1/2}(km)^{-1/4}$ . Two helium isotopes having masses  $m_3 = 3$ ,  $m_4 = 4$  are in amu. Then at the same  $k$  that defines lattice state, the oscillation amplitude ratio equals  $x_{03}/x_{04} = (m_4/m_3)^{1/4} \simeq 1,075$ , and ratio of the atomic volumes will be <sup>1</sup>  $V_{03}/V_{04} = (m_4/m_3)^{3/4} \simeq 1,24$ . This means that the impurity <sup>3</sup>He is the dilatation center in <sup>4</sup>He matrix due to the zero-point oscillations.

A dilatation center has an extra volume  $\Omega_0$ . The dilatation volume  $\Omega_0$  is the main characteristic of a dilatation center in the crystal [4,20]. The dilatation center is an interstitial atom with  $\Omega_0 = V_0$  [4]. For impurity <sup>3</sup>He, the dilatation volume is  $\Omega_{03} \simeq V_{04}(V_{03}/V_{04} - 1) \simeq 0,24V_{04}$ .

Interaction  $U_{int}$  of the dilatation center <sup>3</sup>He with an acoustic wave can be written as  $p\Delta V$ , or better

$$U_{int} = +\Delta p \Delta V. \quad (18)$$

Here  $\Delta V = \Omega_{03}$  is the atomic volume change of the impuriton when driving in areas with low pressure,  $\Delta p = p - p_0$  is the change in pressure as the sound wave passes relative to the equilibrium value  $p_0$ . In the case of a fixed impurity position an interaction would be considerably less. Combining the definition of pressure (3), the stress tensor, modules and generalized Hookes law, we obtain:

$$\Delta p = -\frac{1}{3}(\lambda + 2G) \frac{\partial u_i}{\partial x_i}. \quad (19)$$

Finally, the interaction of the longitudinal wave and impuriton is written in the form:

$$U_{int}(\mathbf{r}, t) = -\frac{1}{3}\Omega_{03}\rho c_i^2 \frac{\partial u_i}{\partial x_i}. \quad (20)$$

It is interesting to compare the structure of the resulting interaction of the impuriton-wave (20) with the appropriate terms in [16,17,18] for vacancies and for electrons in the interaction between the electron and acoustic wave in [25]. In [16,17,18] interaction between vacancions describes the local variation of the

<sup>1</sup> We neglect their own volume of the helium atom ( $R_{He}^{at} \simeq R_H^{at}/2 \simeq 0.025nm \ll x_{04} \simeq a/2 \simeq 0.2nm$ ).

kinetic energy of the lattice vibrations due to the presence of vacancies. This kind of interaction is to be written for the fixed defects.

In [25] hamiltonian contains terms (Fourier components) of the interaction between electronic and acoustic waves, its physical meaning is kinetic energy, multiplied by the small strain tensor. In this case, the impuriton-phonon interaction  $U_{int}$  is in a form (with modules of elasticity) whose physical meaning is the potential elastic energy multiplied by the small strain tensor. Therefore, for the interaction terms in (20) and [25] physical meaning is very similar, despite the differences of objects and methods of preparation: they describe the interaction of sound waves and quantum particles.

To account the interaction with impuritons, Lagrangian (8) for longitudinal wave would be supplemented:  $L = K - (U + \int nU_{int}dV)$ . Here  $n \equiv n(\mathbf{r}, t) = (1/V) \sum_i |f_i(\mathbf{r}, t)|^2$  is the average local concentration of the impuritons,  $i$  is the number of particles in a small volume  $V$  in the classic approach. For a single particle we have  $n(\mathbf{r}, t) \rightarrow |f(\mathbf{r}, t)|^2$ , density of probability for an impuriton in the quantum approach. Then the local density of the impuriton-phonon interaction is

$$L_{int} = -\frac{1}{3}\Omega_{03}\rho c_l^2 \int |f(\mathbf{r}, t)|^2 (\nabla u) dV. \quad (21)$$

Then we need to add term  $\partial L_{int}/\partial u_i = + \int \partial(nU_{int})/\partial u_i dV$  into the wave equation (9). To account the impuriton-wave interaction it is necessary to substitute  $U_{int}$  in the equivalent Schrodinger equation. Then we get a system of equations that describes the interacting impuriton and lattice in solid  ${}^4\text{He}$  in 3D case:

$$\rho \frac{\partial^2 \mathbf{u}}{\partial t^2} - \rho c_l^2 \Delta \mathbf{u} - \frac{1}{3}\Omega_{03}\rho c_l^2 \nabla (|f(\mathbf{r}, t)|^2) = 0; \quad (22)$$

$$\varepsilon_n (-i\nabla) f(\mathbf{r}, t) - \frac{1}{3}\Omega_{03}\rho c_l^2 (\nabla u) f(\mathbf{r}, t) = i\hbar \frac{\partial}{\partial t} f(\mathbf{r}, t). \quad (23)$$

Then, in the case of 1D wave and one impuriton, the system of equations takes the form:

$$\rho \frac{\partial^2 u}{\partial t^2} - \rho c_l^2 \frac{\partial^2 u}{\partial x^2} - \frac{1}{3}\Omega_{03}\rho c_l^2 \frac{\partial}{\partial x} |f(\mathbf{r}, t)|^2 = 0; \quad (24)$$

$$\varepsilon (-i \frac{\partial}{\partial x}) f(\mathbf{r}, t) - \frac{1}{3}\Omega_{03}\rho c_l^2 (\frac{\partial u}{\partial x}) f(\mathbf{r}, t) = i\hbar \frac{\partial}{\partial t} f(\mathbf{r}, t). \quad (25)$$

The wave function satisfies to the normalization condition

$$\int |f(\mathbf{r})|^2 d\mathbf{r} = 1. \quad (26)$$

### 3 Quasiparticles: the Impuriton-Phonon Soliton

#### 3.1 Interaction and Dispersion Relations of Phonon and Impuriton

It should be noted that the phenomenon of the interaction of waves of different physical nature is well known in the fundamental science and is used in technique. In plasma an acoustic and ion-plasma waves interact [26]. In magnets the magnon and phonon quasiparticles interaction gives rise to magnetoacoustic waves and to magnetoacoustic technique [27]. A similar approach is applied to interaction of an electron beam with plasma [26] or with acoustic waves [28,25], the last gives rise to acoustoelectronics. The waves interact most strongly at the intersection points of their dispersion laws, where hybrid waves are generated.

Let us find solution for phonon  $u(\mathbf{r}, t)$  and the impuriton wave function  $f(\mathbf{r}, t)$  as plane traveling wave along the axis  $0x$  (we omit the arguments for shortening):

$$\begin{aligned} f(\mathbf{r}, t) &\rightarrow f_x(x, t) \rightarrow f; & f &= f_{\perp} f(x, t) = f_{\perp} f_0 \exp i(kx - \omega t). \\ \rho_u &= \frac{\partial u(\mathbf{r}, t)}{\partial x}; \\ \rho_u(\mathbf{r}, t) &\rightarrow \rho_u(x, t) \rightarrow \rho_u; & \rho_u &= \rho_u(x, t) = \rho_{u0} \exp i(kx - \omega t). \end{aligned} \quad (27)$$

Presence of the same exponents means that we find solutions close to the intersection point of the dispersion laws. Then after substitution  $f(\mathbf{r}, t)$  in equations (24, 25) we obtain the system:

$$\begin{cases} \frac{\partial^2 \rho_u}{\partial t^2} - c_l^2 \frac{\partial^2 \rho_u}{\partial x^2} - \frac{1}{3} \Omega_{03} c_l^2 |f_\perp|^2 \frac{\partial^2}{\partial x^2} |f_x|^2 = 0; \\ \varepsilon (-i \frac{\partial}{\partial x}) f_x - \frac{1}{3} \Omega_{03} \rho c_l^2 \rho_u f_x = i \hbar \frac{\partial}{\partial t} f_x. \end{cases} \quad (28)$$

All terms that describe interaction are nonlinear in our case. So in linear approximation let us substitute exponents (27) into equations system (28) which splits into two independent dispersion laws:

$$\begin{cases} \omega = c_l k; \\ \hbar \omega = \varepsilon(k). \end{cases} \quad (29)$$

Thus, in the linear case the interaction of phonons and impuritons impossible. Interaction of waves is possible only due to high power terms which cause the amplitudes depend on coordinates (wave packet). Let us consider the consequences of necessity of the envelope waves for the amplitudes.

### 3.2 Equation for Envelope Waves

We find a solution to the impuriton wave function as a wave packet (envelope wave) as in (27) and divide dependencies into two groups in longitudinal and transverse directions. After substituting in equations (24, 25)  $f(\mathbf{r}, t)$  the system of equations is transformed to the form:

$$\begin{cases} \frac{\partial^2 \rho_u}{\partial t^2} - c_l^2 \frac{\partial^2 \rho_u}{\partial x^2} - \frac{1}{3} \Omega_{03} c_l^2 |f_\perp|^2 \frac{\partial^2}{\partial x^2} |f_x|^2 = 0; \\ (\varepsilon_0 + \Delta \varepsilon) f_x - \frac{\hbar^2}{2m^*} \frac{\partial^2}{\partial x^2} f_x - \frac{f_x}{f_\perp} \frac{\hbar^2}{2m^*} \Delta_\perp f_\perp - \frac{1}{3} \Omega_{03} \rho c_l^2 \rho_u f_x = i \hbar \frac{\partial}{\partial t} f_x. \end{cases} \quad (30)$$

This system of equations is very similar to the equations describing electron in an elastic molecular chain [29]. We have the following differences between equations for these physical systems: 1) the sign of the effective mass (is negative here), 2) terms  $\varepsilon_0 + \Delta \varepsilon$  correspond to the level of the energy band top here; 3) the coefficients of the interaction terms are different. These differences reflect the specificities of different physical systems.

The next step is possible for stationary envelope waves with velocity  $V$ :

$$\xi = (x - x_0 - Vt); \quad u(\xi); \quad f_0(\xi); \quad \frac{\partial}{\partial x} = \frac{d}{d\xi}; \quad \frac{\partial}{\partial t} = -V \frac{d}{d\xi}. \quad (31)$$

The imaginary part of the second equation equal zero ( $k = m^*V/\hbar$ ), and we introduce the variables

$$\begin{aligned} s^2 &= \frac{V^2}{c_l^2}; \quad E = W - (E_m + \frac{m^*V^2}{2}); \\ W &= \hbar \omega; \quad E_m = \varepsilon_0 + \Delta \varepsilon + \varepsilon_\perp; \end{aligned} \quad (32)$$

Here  $E_m$  is the band top level for the impuriton accounting transverse energy,  $W$  is the impuriton total energy,  $E$  is the impuriton total energy excluding kinetic energy and measured from the band top. Then the system (30) can be simplified:

$$\begin{cases} (1 - s^2) \frac{d^2 \rho_u}{d\xi^2} + \frac{1}{3} \Omega_{03} |f_\perp|^2 \frac{d^2}{d\xi^2} |f_0|^2 = 0; \\ -\frac{\hbar^2}{2m^*} \frac{d^2}{d\xi^2} f_0 - \frac{1}{3} \Omega_{03} \rho c_l^2 \rho_u f_0 = +E f_0. \end{cases} \quad (33)$$

Now, the first equation can be partially integrated:

$$\rho_u = \frac{du}{d\xi} = -\frac{1}{3} \frac{\Omega_{03} |f_\perp|^2}{1 - s^2} |f_0(\xi)|^2 + C_1 \xi + C_2; \quad (34)$$

Usually the integration constants  $C_1, C_2$  assumed to be zero, because  $\rho_u = 0$  and  $d\rho_u/d\xi = 0$  if  $|f_0(\pm\infty)|^2 = 0$  [29], [30]. After replacing  $\rho_u$  in equation (33b) we obtain nonlinear Schrodinger equation for the impuriton-phonon envelope waves:

$$\frac{d^2}{d\xi^2} f_0 + \varepsilon f_0 - 2g_1 f_0 |f_0|^2 = 0. \tag{35}$$

where we have introduced variables

$$\varepsilon = E \frac{2m^*}{\hbar^2}; \quad g_1 = \frac{1}{9} \rho c_l^2 \frac{\Omega_{03}^2 |f_\perp|^2}{1-s^2} \frac{m^*}{\hbar^2}; \tag{36}$$

It is important to further that  $g_1 < 0$  because  $m^* < 0$ , and  $\varepsilon$  can be both positive and negative.

### 3.3 Envelope Solitary Wave: the Impuriton-Phonon

Integration of the nonlinear Schrodinger equation (35) yields the following soliton solution for the wave function

$$f_0(\xi) = \frac{A}{\cosh(\xi/l_\xi)}. \tag{37}$$

and displacements, according to (34)

$$\rho_u(\xi) = \frac{du}{d\xi} = -\frac{1}{3} \frac{\Omega_{03} |f_\perp|^2}{1-s^2} |f_0(\xi)|^2; \tag{38}$$

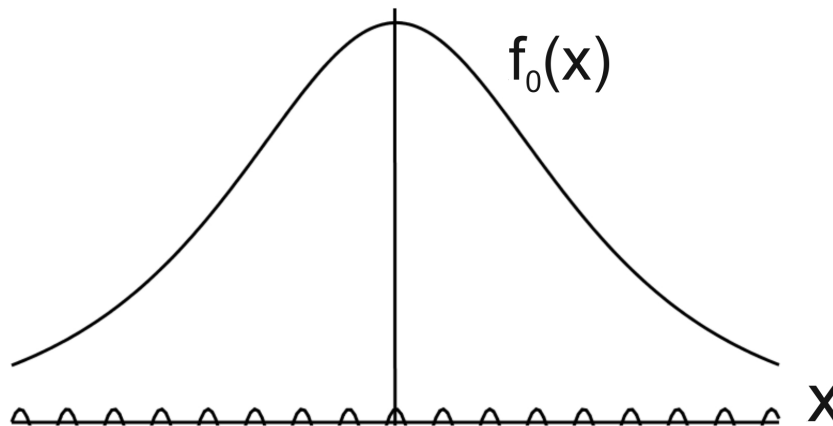


**Figure 1.** The dependence of the wave function  $|f_0(\xi)|$  of the mpuriton-phonon soliton on coordinates (37). Atoms along the x-axis are shown with lattice constant periodicity. The characteristic soliton length  $l_\xi$  is from line 5 in Table 1.

The soliton parameters, the characteristic length and amplitude are

$$l_\xi = \frac{1}{\sqrt{-\varepsilon}}; \quad A = \sqrt{\varepsilon/g_1}; \tag{39}$$

The shape of the wave function (37) is shown in Fig. 1 in comparison with the lattice constant and based on  $l_\xi$  estimation obtained in Table 1 below.

Normalization (26) gives the soliton energy  $E$  depending on velocity  $s$ :

$$E = \frac{E_0}{(1-s^2)^2}; \tag{40}$$

$$E_{thi} = E_0 = -\frac{m^* \rho^2 c_l^4 \Omega_{03}^4}{8 \cdot 81 \pi^2 R^4 \hbar^2};$$

Here  $E_{thi} = E_0 > 0$  is impuriton contribution to the soliton gap (threshold) at  $s = 0$ . Instead of choosing the test wave function  $f_{\perp}(\mathbf{r}_{\perp})$ , as it was done in [30], we introduced  $R$ , the characteristic radius of transvers cross section of the soliton, and step wave function:

$$f_{\perp}(\mathbf{r}_{\perp}) = \begin{cases} 1; & |r_{\perp}| \leq R; \\ 0; & |r_{\perp}| > R. \end{cases} \quad (41)$$

From relations (32) we can find the impuriton-phonon energy dependence on velocity

$$W - E_m = E_0[-bs^2 + \frac{1}{(1-s^2)^2}]; \quad (42)$$

where parameter of the dimensionless impuriton energy is introduced:

$$b = -\frac{m^*c_l^2}{2E_0} > 0. \quad (43)$$

Parameter  $b$  is the impuriton kinetic energy at sound velocity normalized to the soliton gap width.

### 3.4 Soliton Elastic Energy

The impuriton-phonon soliton energy, obtained above, considers impuriton energy and its interaction with lattice. In addition, there is the contribution of an accompanying lattice deformation with Lagrangian  $L = K - U$  (8). Here  $K, U$  are the kinetic and potential energies of the lattice. Hamiltonian  $H = K + U$  determines the elastic energy of the lattice  $E_L$ . Its dependence on  $\xi$  (31) gives the factor  $1 + s^2$ . The explicit form of the function  $du/d\xi$  (38) and the wave function (37), separation of longitudinal and transverse variables simplifies the integral:

$$E_L = \frac{1}{2}\rho c_l^2(1+s^2)\frac{\pi R^2}{9}\left(\frac{\Omega_{03}^2 A^4}{(1-s^2)^2}\right)l_{\xi}\int_{-\infty}^{+\infty}\frac{dy}{\cosh^4 y}. \quad (44)$$

The explicit form of the soliton parameters (39) and simplification give

$$E_L = \frac{2}{3}E_0\frac{1+s^2}{(1-s^2)^3}. \quad (45)$$

where  $E_0$  and  $s^2$  are defined by the relations (40) and (32), respectively.

Thus, to obtain the total energy of the impuriton-phonon soliton it is necessary to summarize the impuriton and elastic parts of the soliton energy:

$$\begin{aligned} E_{i-p}(s) &= W - E_m + E_L; \\ E_{i-p}(s) &= E_0\left(\frac{1}{(1-s^2)^2} + \frac{2}{3}\frac{1+s^2}{(1-s^2)^3} - bs^2\right); \end{aligned} \quad (46)$$

At  $s = 0$  considering the elastic energy the gap for formation of the impuriton-phonon soliton is

$$E_{th} = E_{i-p}(0) = \frac{5}{3}E_0; \quad (47)$$

With elastic energy accounting, the gap becomes larger, however, the result does not change qualitatively. The total energy dependence of the impuriton-phonon soliton on velocity (46) is shown in Fig. 2.

## 4 The Chemical Potential as a Driving Force

In the phase equilibrium their chemical potentials  $\mu_i(T, P)$  are equal [31]. If we change the thermodynamic parameters (temperature, pressure) equilibrium condition breaks: the difference of the chemical potentials

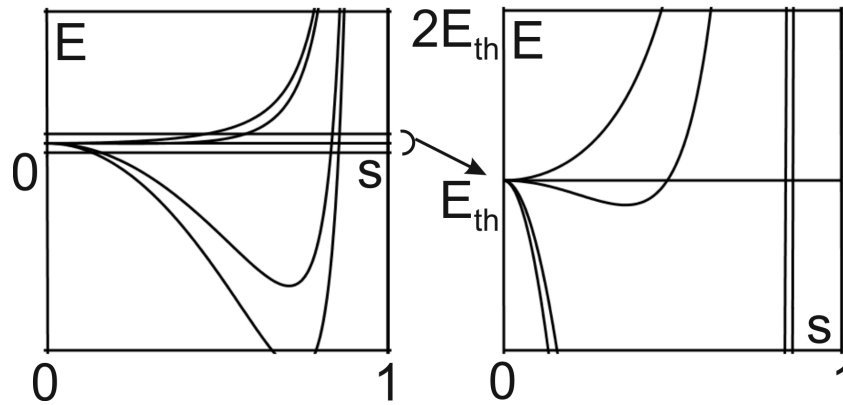


**Figure 2.** Energy of the impuriton-phonon soliton depending on the velocity ( $0 \leq s \leq 1$ ) according to relation (46). When the parameter values are  $b=0; 10; 71.2; 99.8$ , the curves are arranged sequentially downwards. The last two values of  $b$  are obtained from the comparison with experiment, see Table 1. On the left a wide range of energies is depicted. On the right the enlarged fragment  $0 \leq E \leq 2E_{th}$  is shown (on left it is narrow central strip labeled by arc and arrow).

arises between the phases. Then the system reduces its energy by particle transition between phases and  $\mu_i(T, P)$  approach to a new equilibrium.

At fast heating (cooling) during one helium atom transition between the phases, change of the system energy can be written as [9,32]  $\Delta E_{3,4} = \Delta\mu_{3,4}(\Delta T)$ . Here the index 3 corresponds to an  $^3\text{He}$  atom transition from  $^3\text{He}$  nuclei within the  $^4\text{He}$  matrix; the index 4 corresponds to opposite motion of an  $^4\text{He}$  atom. Relation between the chemical potential, temperature and concentration in the  $^3\text{He}-^4\text{He}$  solid solutions was defined [33]. These relations are used in [9,32] for analysis of fast heating from an initial  $T_i$  to a final  $T_f = T_i + \Delta T$  temperature. With the temperature jump the phonon subsystem quickly approaches a new equilibrium, and a new atomic (impurity) equilibrium concentration is reached for a much greater time. In a nonequilibrium state at fast heating due to inconsistencies of  $^3\text{He}$  concentrations, the difference in chemical potential between the states in the nuclei and the matrix appears. The  $^3\text{He}$  atoms concentration is  $X = N_{He3}/(N_{He4} + N_{He3})$ .

According to estimates based on pressure measurement experiments for solid solutions,  $^3\text{He}$  impurity concentration in  $^4\text{He}$  matrix at temperature 100mK is  $X_i^{matr} \simeq (1 \div 28)10^{-5}$ , i.e.  $\ln X_i^{matr} = -(8.2 \div 11.5)$  [32]. Summing the above estimates, at the temperature jump  $\Delta T$  the change in the chemical potential between the phases was written as

$$\Delta\mu_3 \simeq k_B\Delta T \ln X_i^{matr} \simeq -k_B\Delta T(8.2 \div 11.5). \tag{48}$$

Thus, they conclude that at a fixed  $^3\text{He}$  concentration after a temperature jump, the chemical potential change occurs strikingly different in different phases [9,32]. The main contribution to this change results from the matrix phase, depleted by  $^3\text{He}$  isotope. The linear relationship  $\Delta\mu_3(\Delta T)$  (48) is shown in Fig. 3. The jump overheating results a relative decreasing of the  $^3\text{He}$  chemical potential in the matrix.

## 5 Threshold Impuriton-Phonons Generation. Rapid Dissolution Mechanisms

A detailed analysis of the possible transfer mechanisms of  $^3\text{He}$  atoms in different experimental situations was carried out in [32]. Here we consider the  $^3\text{He}$  atom transfer using microscopic model suggested above for impuriton-phonon quasiparticle.

When  $^3\text{He}$  atoms move in the matrix, the particle flux density is as follows:

$$J_m \sim m_3 n_3 v; \tag{49}$$

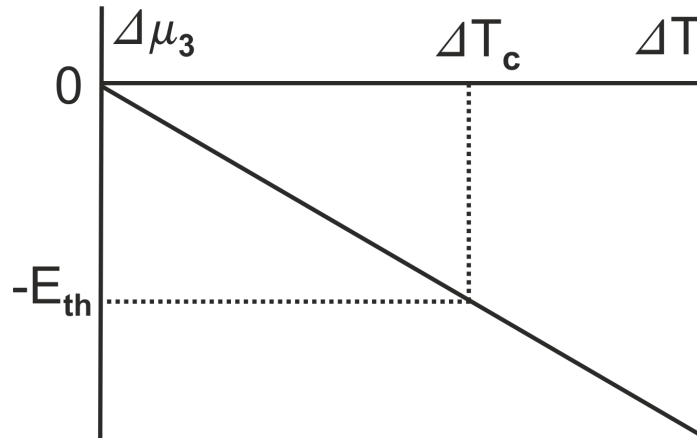


**Figure 3.** The difference between the levels of the chemical potential  $\Delta\mu_3$  in the matrix and in the nucleus depending on the overheating  $\Delta T$  according to relation (48) is shown for the impurity  ${}^3\text{He}$  atoms. Dotted line is overheating threshold  $\Delta T_c$ .

where  $m_3$ ,  $n_3$  are transferred impurity atom mass and their concentration,  $v$  is the average velocity in the flow. The concentration and velocity values change in the space. The initial concentration is determined by complex processes on the nuclear boundary [32]. The relaxation time of the concentration and the pressure is inversely proportional to the flux density:

$$\tau_P \sim \tau_c \sim \frac{1}{J_m} \sim \frac{1}{v}; \quad (50)$$

For small overheating, a bottleneck for the atomic flux value exists, namely, the band movement velocity  $v = v_g$  of the impurity within the matrix (17). When overheating exceeds a threshold value, the average impurity atomic flux increases by orders of magnitude [9,10,11,32].

We attribute this increase in the particle flux to formation the impuriton-phonon quasiparticles (solitons) introduced above. As have been shown, the impuriton-phonon quasiparticle would move at a velocity comparable to the sound speed. The physical meaning of the chemical potential is the energy change of a phase by adding (removing) a particle. Therefore, under overheating the chemical potential change is compatible with following impuriton-phonon energy (see. (46)).

$$\begin{aligned} \mu_3 &= W + E_l; \\ \Delta\mu_3 &= E_{i-p}(s) = \mu_3 - E_m. \end{aligned} \quad (51)$$

At rapid dissolution the threshold formation energy of the impuriton-phonon and the chemical potential change are comparable as follows:

$$\Delta\mu_{3th} = E_{th}. \quad (52)$$

This comparison allows to determine the physical nature of the experimental processes. In case of the overheating, the chemical potential step arises between the nuclei and the matrix  $\Delta\mu_3 < 0$ . Then two mechanisms are possible.

1) **The mechanism I: impuriton and phonon emission and separate motion.**

If  $E_{th} > |\Delta\mu_3(\Delta T_f)|$  i.e. the chemical potential step is lower than the formation energy of the impuriton-phonon quasiparticle, then the impurity atom transition and the impuriton formation must be accompanied by the phonon emission (see Fig. 4a.):

$$|\Delta\mu_3| = \hbar\omega_{ph}(k). \quad (53)$$

Here  $\omega_{ph}(k)$  is the emitted photon frequency (10). Low band velocity of the impuriton movement is the main limiting process of the nuclei dissolution rate. Impuriton just does not have time to leave the nuclei boundary. The nuclei spreading occurs with the impuriton band velocity.

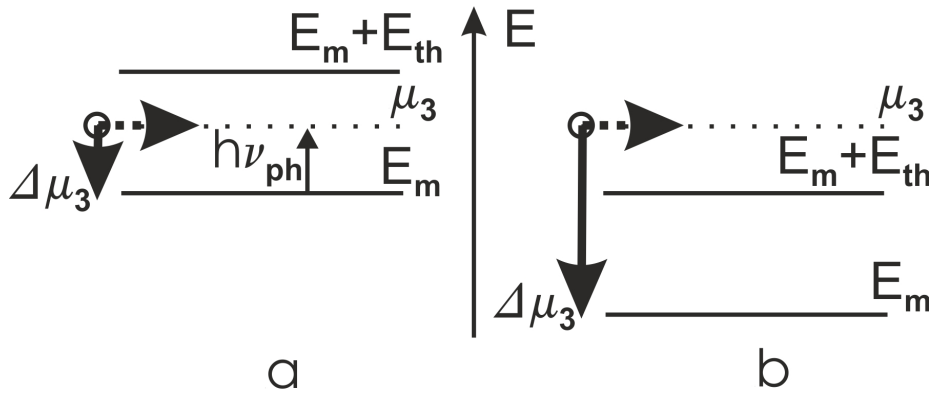


**Figure 4.** The energy levels during an impuriton (circle) transition from the  ${}^3\text{He}$  nucleus in the  ${}^4\text{He}$  matrix at different overheating  $\Delta T$ . The nucleus level (points) of the chemical potential  $\mu_3$  is approximately constant. Heavy vertical arrow from the circle indicates the magnitude and direction of change in the chemical potential in the matrix. Difference  $\Delta\mu_3$  should be compared with a threshold energy  $E_{th}$ , the gap in spectrum of the impuriton-phonon soliton. The heavy horizontal arrow indicates the energy level (51) to which the impuriton falls in the matrix. a) Mechanism 1 at low overheating:  $0 \leq \Delta\mu_3 < E_{th}$ , the emission of a phonon  $h\nu_{ph}$  and further band motion of an impuriton. b) Mechanism 2 for high overheating:  $E_{th} \leq \Delta\mu_3$ , emission of the impuriton-phonon quasiparticle-soliton. See a detailed discussion in the text. In comparison with Fig. 2  $E_{th} \rightarrow E_m + E_{th}$ .

## 2) The mechanism II: the impuriton-phonon quasiparticle emission

At high overheating, the chemical potential step between the nuclei and the matrix begins to exceed (see Fig. 4b.) the threshold energy of the impuriton-phonon soliton formation in the matrix:  $|\Delta\mu_3(\Delta T_f)| \geq E_{th}$ . Inside the matrix after the impurity transition, the impuriton-phonon quasiparticle is formed by combining the properties of impuriton and phonon.

$$\begin{aligned} |\Delta\mu_3(\Delta T_f)| &= E_{i-p}(s) \geq E_{th}; \\ |\Delta\mu_{3th}| &= E_{th}. \end{aligned} \quad (54)$$

Here at the critical overheating  $\Delta T_c$ , jump threshold value of the chemical potential and the soliton energy gap in (47) are equated. Then relation (54) and evaluation  $\Delta\mu_3 = 25\text{m}\hat{\text{E}}$  in (48) make it possible to evaluate the magnitude of the impuriton-phonon soliton gap:

$$E_{th} = k_B \Delta T_c \ln X_i^{matr} \simeq (0, 205 \div 0, 288)K = (0, 283 \div 0, 397) \cdot 10^{-23}J. \quad (55)$$

These estimates are used in Table 1 to evaluate other parameters of the impuriton-phonon soliton.

The impuriton-phonon quasiparticle velocity is comparable to the sound speed  $s \sim 1$  (40). This could explain the anomalously high rate of the  ${}^3\text{He}$  phase nuclei dissolution at overheating above the threshold in the experiment [9]. The impuriton-phonon quasiparticle energy coincides with the chemical potential step at the phase boundary (see Fig. 2, Fig. 3). At low overheating in the first mechanism, the velocity is 5-6 orders of magnitude smaller, so the graph does not differ from zero. The obtained dependence of the velocity of the impuriton and the impuriton-phonon on the overheating value qualitatively agrees with the experimental results in the dissolution rate of the  ${}^3\text{He}$  nuclei. At least a threshold value of high velocity and its dependence on the overheating value appear in the proposed model.

Simultaneous the impuriton formation with the phonon emission, considered in the mechanism 1, is not excluded. Such impuritons formation would lead to a rising smoothing nucleus-matrix boundaries and termination of the impuriton-phonon generation in the long run.

## 6 Photoelectric Effect Analogy

Let us discuss photoelectric effect analogy with the generation of the phonons and the impuriton-phonon quasiparticles. Einsteins photoelectric equation [5]:

$$h\nu = \phi + \frac{mV^2}{2}, \quad (56)$$

involves the energy of an incident photon  $h\nu$ , work function  $\phi$ , and kinetic energy  $mV^2/2$  of the emitted photoelectron.  $h$  is Planck's constant.

Equation for the impuriton-phonon soliton (46) has similar structure:

$$E_{i-p}(s) = W - E_m + E_l = E + E_l + \frac{m^*V^2}{2}; \quad (57)$$

For more similarity with the Einsteins equation we can write this relation in the following form

$$\begin{aligned} |\Delta\mu_3(\Delta T_f)| &= E_{th} + E_{sm} + \frac{m^*V^2}{2}; \\ E_{sm} &= (E + E_l - E_{th}); \end{aligned} \quad (58)$$

where the explicit dependence of the energy  $(E + E_l) + mV^2/2$  on velocity is given by (46). The terms have the following meanings.  $W - E_m \equiv |\Delta\mu_3(\Delta T_f)|$  is the impuriton total energy measured from the band top.  $E_{th}$  is gap in the impuriton-phonon soliton spectrum.  $E_{sm}$  is the smooth part of the soliton spectrum above the gap.  $mV^2/2$  is kinetic energy of an impuriton emitted from the impuriton band.

Both equations express the energy conservation law in the interaction of particles (quasiparticles) with matter. All terms in the equations (56), (58) can be mapped with each other:

$$\begin{cases} \hbar\omega & \leftrightarrow |\Delta\mu_3|; \\ \phi & \leftrightarrow E_{th}; \\ \frac{mV^2}{2} & \leftrightarrow E_{sm} + \frac{mV^2}{2}. \end{cases} \quad (59)$$

The physical meaning of the terms in these equations is very close.

The left side in (56,58) and the first line in (59) contain the initial high-energy particle (step height from which the particle falls). In eq. (58) it is an  $^3\text{He}$  atom heated in a nucleus. In eq. (56) it is photon incident on a metal.

The first term on the right side of the equations (58, 56) and the second line in (59) contain work that must be expanded on particle ejection. In equation (58) it is  $E_{th}$ , the impuriton-phonon spectrum threshold. In equation (56) it is electron work function.

The second term on the right side in the equations (58, 56) and in the third line in (59) contain kinetic energy of the emitted particle. In equation (58), it is the impuriton-phonon soliton energy above the gap plus the kinetic energy of the emitted impuriton. In equation (56), it is the kinetic energy of the emitted electrons.

In the right-hand side of equation (56), the only particle, electron, start move over the potential step (the work function). After critical overheating, the only particle is emitted: the impuriton-phonon above the soliton energy gap.

**The photoelectric threshold energy** can be obtained from the Einsteins photoelectric equation if the electron velocity  $V$  is zero. Velocity of the emitted impuriton-phonon plays the same role. **The impuriton-phonon emission threshold** can be found by substituting zero velocity. Then, in the photoelectric effect and in the impuriton-phonon emission the threshold energy can be written in the same form:

$$\begin{aligned} \hbar\omega_{th} &= \phi; \\ |\Delta\mu_{3th}| &= E_{th}. \end{aligned} \quad (60)$$

where the energy threshold  $E_{th}$  of the soliton formation is given by relations (47) and (55).

## 7 Results and Comparison with Experiment

### 7.1 Estimation of the Parameters

Discussion of the results we start by estimation of the parameters of the impuriton-phonon soliton, namely, the effective mass  $m^*$ , the effective length  $l_\xi$ , the effective radius  $R$ , the normalizing factor  $b$  of the

impuriton-phonon kinetic energy from the relations (13), (39), (40), (47), respectively. To estimate these parameters we use the experimental values from [34]. For hcp  ${}^4\text{He}$  the numerical value of the molar volume is  $V_m=20.97\cdot 10^{-6}\text{m}^3/\text{mol}$ . Atomic mass is  $m_a \simeq 6,68\cdot 10^{-27}\text{kg}$ . Atomic volume  $V_{04}$  can be estimated from the molar volume  $V_m$  for helium  $V_{04} = V_m/N_A \simeq 3,48\cdot 10^{-29}\text{m}^3$ . For the impurity  ${}^3\text{He}$  atom the effective mass is  $m^* = -m_{04}/4 = -1.67\cdot 10^{-27}\text{kg}$  according to (13) and  $\Omega_{03} \simeq 0.24V_{04} = 8,36\cdot 10^{-30}\text{m}^3$ . Density is  $\rho = \mu/V_m = 191\text{kg}/\text{m}^3$  where  $\mu$  is  ${}^4\text{He}$  molar mass. The longitudinal sound velocity is  $c_l \simeq 450\text{m}/\text{s}$ .

All estimates of the parameters of the impuriton-phonon soliton are given in Table 1. The first and second (third) columns of the Table 1 are the effective mass and the width of the impuriton band related by (13). In line 1 the effective mass and the impuriton band width are shown. In lines 2 and 4, it was assumed that the impuriton band expands to the value of the soliton gap  $\Delta\varepsilon = E_{th}$  when the impuriton-phonon is formed. In Table 1 before lines 1 and 4  $E_{th}$  values are obtained from the analysis of the chemical potential behavior in the experiment (55). In lines 3 and 5 the effective mass is assumed to be negative (minus one amu, the difference between the atomic masses of  ${}^3\text{He}$  and  ${}^4\text{He}$  isotopes), it is mass of the free particle (hole). The effective mass reduces if the band expands on.

**Table 1.** The calculated parameters of the impuriton-phonon soliton for the overheating  $\Delta T=25\text{mK}$ . Estimates are carried out for the effective mass  $m^*$ , the effective length  $l_\xi$ , effective radius  $R$  and the normalization factor  $b$  of the impuriton kinetic energy. For the discussion see text.

N	$-m, \text{kg}$	$\Delta\varepsilon, \text{K}$	$\Delta\varepsilon, \text{J}$	$\frac{l_\xi}{1-s^2}, \text{\AA}$	$R, \text{\AA}$	$b$
1	2	3	4	5	6	
$E_{th}=0,21 \text{ K}$						
1	$6,58\cdot 10^{-23}$	$10^{-4}$	$1,38\cdot 10^{-27}$	$4,62\cdot 10^{-2}$	11,42	$1,68\text{\AA}\cdot 10^6$
2	$3,21\cdot 10^{-26}$	0,21	$2,83\cdot 10^{-24}$	$a/\sqrt{2}$	1,85	1ă149
3	$1,67\cdot 10^{-27}$	–	–	13,9	1,00	99,8
$E_{th}=0,29\text{K}$						
4	$2,29\cdot 10^{-26}$	0,29	$3,97\cdot 10^{-24}$	$a/\sqrt{2}$	1,56	584
5	$1,67\cdot 10^{-27}$	–	–	11,8	0,92	71,2

The effective length  $l_\xi$  of the impuriton-phonon soliton (39) is calculated according to effective mass and energy of a soliton  $E$  (36). It is 4th column of the Table 1. The largest effective length of the soliton  $l_\xi \simeq 10\text{\AA}$  is obtained in lines 3 and 5 of the Table 1 for free particles. This solution is in agreement with the chosen research approach of monochromatic oscillations modulated by slowly varying amplitudes. For the rest masses (lines 1, 2 and 4) the effective length of the soliton is less than lattice period  $a$ , which does not meet the model under investigation. Thus, in the case of the band movements (line 1) the soliton length is several orders smaller than the lattice period. Now, therefore, the soliton characteristic size is  $\simeq 2l_\xi \simeq 24 - 28\text{\AA}$  plus the exponential tails. The characteristic length reduces with factor  $(1-s^2)$  when velocity is increasing. The shape of the wave function (37) in comparison with the lattice constant is shown in Fig. 1.

The effective radius  $R$  of the impuriton-phonon soliton (the fifth column of the Table 1) is calculated according to value of the gap soliton formation  $E_0$  (40) and the effective mass (the same line). For free particle (lines 3, 5) we have  $R \simeq 1\text{\AA}$  (plus the exponential tails) i.e. the soliton transverse dimension is order of atomic size.

Parameter  $b$  (sixth column of the Table 1) is calculated according to the radius  $R$  value. We can see from this relationship that the parameter  $b$  decreases with increasing effective mass and the impuriton-phonon soliton radius. For the obtained parameter  $b$  values (in Table 1) the total energy of the impuriton-phonon soliton dependence on velocity (46) is shown in Fig. 2.

## 7.2 Experiment and Velocity of the Impuriton-Phonon Soliton

The parameter  $b$  allows to find the impuriton-phonon soliton velocity shown in Fig. 2. To find corresponding to experiment, we transform Fig. 2, arrange it close to the experimental data plot and make equal scale of horizontal axis, see Fig. 5.

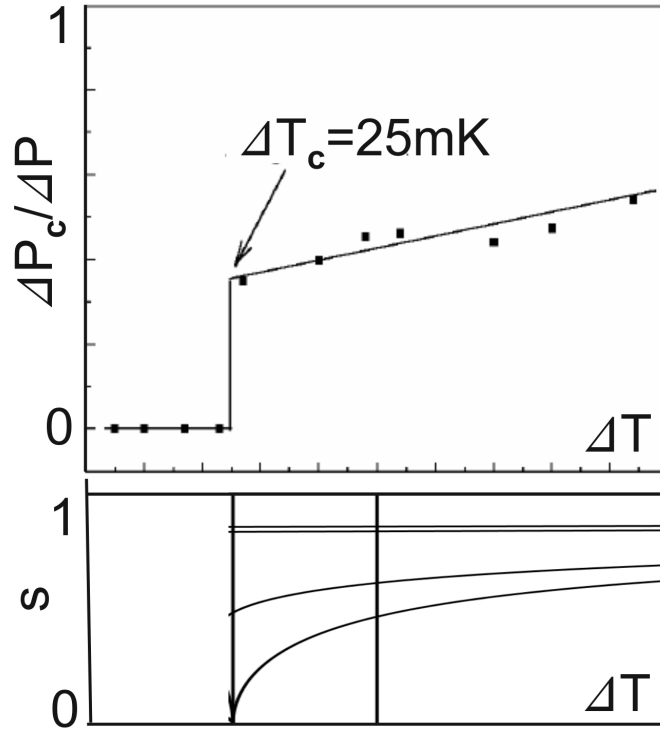


**Figure 5.** Comparison of the experimental (top panel) and the theoretical (bottom panel) results. Top (upper panel) shows the dependence of the relative pressure jump (dissolution rate) on the overheating value  $\Delta T$  in the  $^3\text{He}$ - $^4\text{He}$  system. Bottom (lower panel) shows dependence of velocity on the energy of the impuriton-phonon quasiparticle according to (46).

Top (upper panel) in Fig. 5 shows the experimentally measured value of the pressure jump ( $\Delta P$ ) should linear depend on the overheating value.

Bottom (lower panel). In view of the proportionality of  $E \sim \Delta\mu_3 \sim \Delta T$  the values ( $T = 0$ )- ( $E = 0 \rightarrow E_m$ ) and  $T_c - E_{th} \rightarrow E_m + E_{th}$  are combined. In comparison with Fig. 2, the axes are rotated  $90^\circ$ , the subthreshold part is removed, the area above the threshold (to the right of the vertical lines) is extended to cover the experimental  $\Delta T$  range. The horizontal line  $s = 1$  is velocity of sound. Below, two almost parallel horizontal curves  $s(E)$  are built based on the experimental data with  $b=71.2$ ;  $99.8$  from Table 1.

At these curves the velocity magnitude is  $s = V/c_l \simeq 0,8$ . At lower value of the parameter  $b$  a curved shape of the experimental curve can be approximated. However, the decrease in pressure jump near the threshold can be associated with a hysteresis (unstable) regime change for particle emission mechanism  $1 \rightarrow 2$  with  $\Delta T$  increasing.

The average values of the experimental dependence  $\Delta p(\Delta T)$  over the threshold we approximate these curves while magnitude of the velocity is  $s = V/c_l \simeq 0,8$ . At lower value of the parameter  $b$  a curved shape of the experimental curve can be approximated in the top panel. However, the decrease in pressure jump near the threshold can be associated with a delay when the hysteresis (unstable) regime change particle emission mechanism  $1 \rightarrow 2$  with an increase in  $\Delta T$ .

Result of these estimations of the impuriton-phonon soliton parameters leads to the following conclusions. Self-consistency of the approach and calculated parameters is possible only in the case of free

or wide-band motion of the impuriton-phonon. In this case, the resulting characteristic length of the soliton is  $2l_{xi} \simeq 22\text{-}28\text{\AA}$ . In other cases (band motion impuriton) the soliton characteristic length is comparable to the lattice period:  $l_{xi} \simeq a$  (or even less), i.e. envelope waves are not formed. Thus, the applicability of the proposed model is defined by a single parameter, a sufficiently large characteristic length of the soliton. In the case of the large soliton lengths the transverse dimension  $R$  is comparable to atomic size. If we accept a smooth change in the transverse dimensions (as in [30]), then the exponential tails appear, but the situation has not fundamentally changed. This produced unusual geometry for the impuriton-phonon solutions needs further discussion.

### 7.3 Comparison of the Possible Impuriton Physical Models

In SubSect. 7.1 we have obtained the expected result: the applicability of the model requires too large the soliton characteristic size  $l_{xi}$ . This in turn requires too light effective mass and wide band. It should be noted that the impuriton zone cannot describe the rapid movement neither any impuriton nor an impuriton-phonon. The resulting movement of the impurity atoms differs from the previously known slow band motion (12) [2,4]. Here we'll discuss this conflict. Band motion is related with atomic exchange and tunneling between the nearest- neighbor. The best conditions for exchange interaction are created by the atoms arranged at a minimum in distance, i.e., in the close-packed planes in the close-packed directions. Obviously, at the atomic arrangement the impuriton movement with high velocity observed experimentally is difficult.

The resulting quasiparticles, the impuriton-phonon solitons, have a spindle shape: they are strongly elongated along the direction of motion, states extend tens of interatomic distances and have a small cross-section. It is interesting to note that the obtained geometry of the solutions, the impuriton-phonons, is similar to the one-dimensional crowdion [4]. Crowdion moves in the close-packed planes in the close-packed directions. In this respect, crowdion is similar to the impuriton in band. But in crowdion an individual atom is shifted only for the lattice period. However an impuriton-phonon and an impuriton in band move an individual atom over long distances.

In addition, the geometry of the solutions, the impuriton-phonons, is similar to motion of a channeling particle [35]. Apparently, the impuriton-phonons as well as the channeling particles more easily move in less densely packed planes in less densely packed areas, between the crystal planes. A lattice distortion in a loose channel for impuriton creates conditions for a simultaneous phonon channeling. Conditions of phonons channeling are considered in [36,37]. It seems that analogy between the impuriton-phonon quasiparticle and a channeling particle is the most adequate.

It should be noted that the theory was originally built around the idea  $^3\text{He}$  atom movement in impuriton band. However, the parameters estimation demonstrated that impuriton-phonon soliton moves out of a band in the sense of conventional  $^3\text{He}$  impuriton. The condition of applicability of the soliton description (envelope wave) necessarily requires a relatively large soliton characteristic length. The latter condition is satisfied only for small effective mass in comparison to the band movement. That is, avoiding movement in the impuriton band is accompanied by movement in a wide band with a small impuriton effective mass. A departure from an impuriton band motion results in the movement in the wide band with a small impuriton effective mass. The indicated process can not occur without changes in an impuriton motion and interaction in direct space. This fact is reflected in the discussed above relatively loose channel for the impuriton-phonon motion.

It is possible, estimation of the volume energy density inside the impuriton-phonon soliton will promote understanding in choosing the rapid dissolution model. During the transition into the matrix, impuriton emits energy  $\Delta\mu_3 \simeq k_B\Delta T \ln X_i^{matr}$  (48) (as phonon or impuriton-phonon quantum) reached at critical overheating  $\Delta T \geq \Delta T_c=25\text{mK}$ . The soliton volume according to its parameters is  $V \simeq 2\pi R^2 l_\xi \simeq (74 \div 87) \cdot 10^{-30} m^3$ . Then the minimum volume energy density inside the impuriton-phonon soliton is

$$w_{min} \simeq \frac{W}{V} \simeq (3 \div 5) \cdot 10^{+4} \left( \frac{J}{m^3} \right).$$

As we can see in Fig. 5 the experimental overheating value can reach  $\simeq 4\Delta T_c$ , in the further experiments  $\simeq 8\Delta T_c$ . So volume energy density can be considerably higher. In the center of the soliton the energy density can be several times more. At found energy densities, it is possible to change as the channeling

conditions as tunneling with impuriton band expansion (phonon assisted tunneling, deformation potential etc.).

#### 7.4 The Generation Mechanisms

Let us discuss how the proposed mechanisms for generation of the impuriton-phonon quasiparticle or phonon and impuritons (see Sect. 5) can demonstrate themselves in the experiment. So, the mechanisms described in the dissolution of the  $^3\text{He}$  nuclei with increasing overheating value  $\Delta T$  are realized in the following order: 1) the mechanism of emission impuritons and phonons separately, 2) the impuriton-phonon emission.

The dissolution of nuclei may start with 2nd mechanism (generation of the impuriton-phonon quasiparticles) if a sufficiently high initial overheating, which exceeds the threshold value  $|\Delta\mu(\Delta T)| \geq E_{th}$ , will be created. With time the impurity  $^3\text{He}$  concentration increases in the matrix as far as the nucleus dissolution continues. This increase in concentration causes a decrease in chemical potential difference between the phases, and conditions are created for the consistent implementation of mechanisms 2→1. In other words, when there is a large initial overheating the dissolution mechanism 2 with emission of the impuriton-phonon quasiparticles having velocity comparable to the velocity of longitudinal sound  $c_l$  in the matrix take place. In the matrix the impurity concentration  $^3\text{He}$  leveled in the characteristic time  $\tau_2 \simeq L/v_2 \sim L/c_l$ , where  $L$  is the distance between the nuclei. After the impurity concentration increasing the difference between the chemical potential in the nucleus and in the matrix is reduced to a value  $|\Delta\mu| \leq E_{th}$ . Then the mechanism 1 of nucleus dissolution starts with the separate emission of phonons and impuritons. The impuritons have a band velocity  $v_g \sim 10^{-4}\text{m/s}$  (17), which results the characteristic time  $\tau_1 \simeq L/v_g$ . Thus, when a high initial overheating nuclei, the dissolution mechanisms 2→1 are implemented consistently with the following relation of the characteristic times  $\tau_1 \gg \tau_2$ .

Moreover, the total time  $t_e$  of the impuriton-phonon and impuritons emission depends on the overheating magnitude. It can be assumed that the emission time is proportional to the overheating magnitude. Then the mass  $M_3$  transferred with the rapid nucleus dissolution of the  $^3\text{He}$  phase can be estimated as

$$M_3 \sim JS\tau_2 \rightarrow m_3 \int_0^{\tau_2} v(t)n(t)S(t)dt; \quad (\Delta T > \Delta T_c). \quad (61)$$

where  $J$  and  $S$  can be considered at the surface of a nucleouse.

Both  $n, S$  decrease from an initial to the critical values  $n_0 \rightarrow n_c = 0, S_0 \rightarrow S_c \rightarrow 0$  at which the impuriton-phonon emission is terminated because of chemical potential step reaches the threshold value. We can suppose  $\tau_2$  or some combination of  $\tau_2$  and  $n$  to be linearly dependent on overheating  $F(n, \tau_2) \sim \Delta T$ . It can improve understanding of correlation of experimental and theoretical results in Fig. 5.

In our opinion the proposed nuclei dissolution scheme describes qualitatively the experimentally observed situation [9,32]. The model describes the following experimental features. 1. For the rapid nucleus dissolution mechanism (the impuriton-phonon quasiparticles emission) the threshold behavior is explained and dependence of the dissolution rate on overheating is obtained qualitatively (more precisely, the particle velocity dependence on the overheating is obviously obtained). 2. transformation of rapid into slow dissolution after a certain alignment time (leveling time) which is not detect in the experiment.

From a comparison with experiment the initial impuriton-phonons velocity depending on overheating above a threshold is to be determined. This parameter is directly related to the excitation threshold of the impuriton-phonons and the critical overheating. Because of the complex geometry and a large number of other factors, the impuritons velocity itself is not obtained in the experiment with rapid dissolution of the  $^3\text{He}$  nuclei. So far only a qualitative comparison of the experimental data with the theoretical results of this work is possible.

## 8 Conclusion

The following systems have been considered: the pure  $^4\text{He}$  matrix with phonons and the isotopic impurity  $^3\text{He}$  atoms (impuritons). The interaction of impuritons and phonons has been introduced and analyzed.

This interaction has been written using dilatation volume and the sound wave pressure. The system of equations that describes the interaction of phonons and the impuritons has been derived. The system includes the wave equation for the phonons interacting with the impuritons and the Schrodinger equation for the impuritons interacting with phonons. The analysis shows that the interaction of the waves occurs only if an impuritons wave packet exists, ie, the problem is essentially nonlinear. For the envelope waves the system has been reduced to a nonlinear Schrodinger equation which has a soliton solution, the impuriton-phonon quasiparticle. The normalization condition for the impuriton wave function determines its energy dependence on the velocity and the transverse dimension of the impuriton-phonon. Due to the negative impuriton mass, velocity dependence on the impuriton-phonon energy is S-shaped that corresponds to the threshold dependence of the  $^3\text{He}$  nucleous dissolution rate on overheating in the experiment. Analogy with the photoelectric effect has been introduced. The threshold overheating temperature (chemical potential jump) has been responded to threshold in the photoelectric effect. It is shown that the narrow impuriton band cannot describe the rapid movement of the impuriton-phonon quasiparticle; alternative descriptions, channeling and induced transformation of the band, are proposed. The velocity dependence on energy and accounting of the soliton gap magnitude allow us to estimate the impuriton-phonon velocity  $v \simeq 0.8c_l$  and qualitatively reproduce the experimental dependence of the nucleous dissolution rate on the overheating.

**Acknowledgments.** We thank colleagues of department of quantum liquids and crystals B.I.Verkin ILTPE NASU, for useful discussions of the experiment. This research is supported by grant #4/17-N of National Academy of Sciences of Ukraine and the Project M0624 of Ministry of Science and Education of Ukraine.

## References

1. S. B. Trickey, W. P. Kirk, and E. D. Adams, "Thermodynamic, elastic, and magnetic properties of solid helium," *Reviews of Modern Physics*, vol. 44, no. 4, p. 668, 1972.
2. A. F. Andreev and I. M. Lifshitz, "Quantum theory of crystal defects," *Sov. Phys. JETP*, vol. 29, p. 1107, 1969.
3. V. N. Grigor'ev, "Impuritons detection in solid helium," *Sov. Journ. Low Temp. Phys.*, vol. 1, no. 1, p. 227, 1975.
4. A. M. Kosevich, *The crystal lattice: phonons, solitons, dislocations, superlattices*. John Wiley & Sons, Weinheim, 2006.
5. C. Kittel, *Introduction to Solid State Physics*. John Wiley & Sons, 2004.
6. R. A. Guyer, R. C. Richardson, and L. I. Zane, "Excitations in quantum crystals (a survey of nmr experiments in solid helium)," *Reviews of Modern Physics*, vol. 43, no. 4, pp. 532–600, 1971.
7. A. F. Andreev, "Diffusion in quantum crystals," *Soviet Physics Uspekhi*, vol. 19, no. 2, p. 137–148, 1976.
8. V. N. Grigor'ev, "Diffusion in solid helium (a review)," *Low Temperature Physics*, vol. 23, no. 1, pp. 3–14, 1997.
9. V. Maidanov, A. Ganshin, V. Grigor'ev, N. Omelaenko, A. Penzev, E. Rudavskii, and A. Rybalko, "Kinetics of dissolution of the  $^3\text{He}$  inclusions in solid  $^4\text{He}$ ," *Physica B: Condensed Matter*, vol. 284, pp. 371–372, 2000.
10. A. N. Gan'shin, V. N. Grigor'ev, V. A. Maidanov, N. F. Omelaenko, A. A. Penzev, E. Y. Rudavskii, A. S. Rybalko, and Y. A. Tokar, "Growth and dissolution kinetics of  $^3\text{He}$  inclusions in phase-separated  $^3\text{He}$ - $^4\text{He}$  solid mixtures," *Low Temperature Physics*, vol. 25, pp. 592–606, 1999.
11. A. Ganshin, V. Grigor'ev, V. Maidanov, P. A. Omelaenko, N., E. Rudavskii, and A. Rybalko, "Threshold effect during dissolution of  $^3\text{He}$  inclusions in solid  $^4\text{He}$ ," *Journal of low temperature physics*, vol. 116, no. 5-6, pp. 349–357, 1999.
12. Y. Kagan and L. A. Maksimov, "Theory of particle transfer in extremely narrow bands," *Zhurnal Eksperimental'noj i Teoreticheskoy Fiziki*, vol. 65, no. 2, pp. 622–632, 1973.
13. Y. Kagan, "Quantum diffusion in solids," *Journal of Low Temperature Physics*, vol. 87, no. 3, pp. 525–569, 1992. [Online]. Available: <http://dx.doi.org/10.1007/BF00114916>
14. V. A. Lykah and E. S. Syrkin, "Quantum behavior of the twin boundary and the stacking fault in hcp helium crystals," *Journal of Low Temperature Physics*, vol. 181, no. 1-2, pp. 10–29, 2015.
15. O. Pelleg, J. Bossy, E. Farhi, M. Shay, V. Sorkin, and E. Polturak, "Opticlike excitations in bcc  $^4\text{He}$ : An inelastic neutron scattering study," *Physical Review*, vol. B 73, no. 18, p. 180301(R), 2006.
16. J. H. Hetherington, "Formation of nonlocalized vacancies in bcc  $^3\text{He}$ ," *Physical Review*, vol. 176, no. 1, pp. 231–238, 1968.

17. R. A. Guyer, "Vacancy waves," *Journal of Low Temperature Physics*, vol. 8, no. 5-6, pp. 427–447, 1972.
18. A. F. Andreev, "Quantum crystals," *Progress in Low Temperature Physics*, vol. 8, pp. 67–131, 1982.
19. V. A. Mikheev, B. N. Eelson, V. N. Grigor'ev, and N. P. Mihin, "Detecting of impuritons scattering on phonons in solid helium," *Soviet Journal Low Temperature Physics*, vol. 3, pp. 386–388, 1977.
20. L. D. Landau, E. M. Lifshits, and L. P. Pitaevskii, *Theory of Elasticity*. Pergamon Press, New York, 1986.
21. A. M. Kosevich, Y. A. Kosevich, and E. S. Syrkin, "Generalized rayleigh waves and the geometry of isofrequency surfaces of sound oscillation waves in crystals," *Zhurnal Eksperimental'noj i Teoreticheskoy Fiziki*, vol. 88, no. 3, pp. 1089–1097, 1985.
22. Y. A. Kosevich and E. S. Syrkin, "Existence criterion and properties of deeply penetrating rayleigh waves in crystals," *Zhurnal Eksperimental'noj i Teoreticheskoy Fiziki*, vol. 89, no. 6, pp. 2221–2229, 1985.
23. J. M. Ziman, *Principles of the Theory of Solids*. Cambridge university press, 1972.
24. I. M. Lifshitz, M. Y. Azbel, and M. I. Kaganov, *Electron Theory of Metals*. Consultants Bureau, New York, 1973.
25. G. L. Bir and G. E. Pikus, *Symmetry and deformation effects in semiconductors*. Nauka, Moscow (in Russian), 1972.
26. P. M. Platzman and P. A. Wolff, *Waves and interactions in solid state plasmas*. Academic Press, 1973.
27. A. G. Gurevich and G. A. Melkov, *Magnetization oscillations and waves*. CRC press, 1996.
28. Y. V. Gulyaev and F. S. Hickernell, "Acoustoelectronics: History, present state, and new ideas for a new era," in *Ultrasonics Symposium, 2004 IEEE*, vol. 1. IEEE, 2004, pp. 182–190.
29. A. S. Davydov, *Solitons in molecular systems*. Springer Netherlands, 1984, vol. 1.
30. A. N. Bugay and S. V. Sazonov, "Electrical solitons in molecular chains, taking into account the higher spatial dimensions," *Theoretical Physics*, vol. 9, pp. 86–92, 2008 (in Russian).
31. L. D. Landau and E. M. Lifshits, *Statistical Physics*. Oxford: Pergamon Press, 1980, vol. 1.
32. A. A. Penzev, *Phase diagram and mass transfer at the separation in solid solutions of helium isotopes*. PhD Thesis, Kharkov, 141 p. (in Russian), 2003.
33. D. O. Edwards and S. Balibar, "Calculation of the phase diagram of  $^3\text{He}$  -  $^4\text{He}$  solid and liquid mixtures," *Physical Review B*, vol. 39, no. 7, pp. 4083–4097, 1989.
34. D. S. Greywall, "Elastic constants of hcp  $^4\text{He}$ ," *Physical Review B*, vol. 16, no. 11, pp. 5127–5128, 1977.
35. U. I. Uggerhøj, "The interaction of relativistic particles with strong crystalline fields," *Reviews of modern physics*, vol. 77, no. 4, pp. 1131–1171, 2005.
36. W. Eisenmenger, "Phonon imaging," *Le Journal de Physique Colloques*, vol. 42, no. C6, pp. C6–201, 1981.
37. A. G. Every, G. L. Koos, and J. P. Wolfe, "Ballistic phonon imaging in sapphire: Bulk focusing and critical-cone channeling effects," *Physical Review B*, vol. 29, no. 4, pp. 2190–2209, 1984.